

## Quantitative microscopy of magnetic domains in Fe(100) by core-level x-ray photoelectron spectroscopy

S. Schmidt,<sup>1</sup> N. Weber,<sup>2</sup> H.-J. Elmers,<sup>3,\*</sup> F. Forster,<sup>1,†</sup> F. Reinert,<sup>1,†</sup> S. Hüfner,<sup>1</sup> M. Escher,<sup>2</sup> M. Merkel,<sup>2</sup> B. Krömker,<sup>4</sup> and D. Funnemann<sup>4</sup>

<sup>1</sup>*Experimentalphysik FR 7.2, Universität des Saarlandes, D-66041 Saarbrücken, Germany*

<sup>2</sup>*Focus GmbH, 65510 Hünstetten-Görsroth, Germany*

<sup>3</sup>*Institut für Physik, Universität Mainz, D-55128 Mainz, Germany*

<sup>4</sup>*Omicron Nano Technology GmbH, D-65232 Taunusstein, Germany*

(Received 4 May 2005; published 15 August 2005)

We present an experimental technique for imaging of magnetic domain patterns based on element-specific core-level photoemission using polarized soft-x-ray radiation. It is applied to the measurement of domain patterns at the Fe(100) surface and at the surface of polycrystalline Fe. Different from well established imaging techniques that use a photoemission electron microscope to measure the secondary electron intensity at the Fe absorption threshold, we have investigated the photoemission intensity contrast on the the Fe  $2p_{3/2}$  core level using circularly polarized x-ray light. The linear and circular dichroism characteristics of the identical domain pattern are extracted by linear combinations of the photoemission yield with left and right circular polarization. For the measurement, a newly developed imaging x-ray photoelectron spectroscopy spectrometer “NanoESCA” was used. The method allows, in principle, the determination of all three magnetization components.

DOI: [10.1103/PhysRevB.72.064429](https://doi.org/10.1103/PhysRevB.72.064429)

PACS number(s): 75.70.Kw, 68.37.Xy, 75.50.Bb, 75.70.Rf

### I. INTRODUCTION

Imaging of magnetic domains is fundamental for the increase of knowledge of micromagnetic phenomena.<sup>1</sup> Photoelectron emission microscopy (PEEM) has been used for many years for imaging magnetization structures<sup>2</sup> and is one of the most promising methods for imaging magnetic domains both at high lateral resolution and on a short time scale due to the parallel imaging technique.<sup>3,4</sup> The most widely employed technique for obtaining magnetic contrast is the x-ray magnetic circular dichroism (XMCD) in absorption.<sup>5–7</sup> Electrons are excited from core levels into the unoccupied spin-split valence states by circularly polarized x-ray photons.<sup>8</sup> The initially excited electrons are converted into a large number of secondary electrons that can be used for PEEM imaging without energy filtering.<sup>9,10</sup> However, the absorption depends on the relative orientation of the polarization vector and the magnetization direction and therefore only the magnetization component parallel to the polarization vector is determined.<sup>2</sup>

In our approach, we take advantage of a newly developed apparatus that combines a PEEM with an electron energy filter providing an energy resolution of 110 meV.<sup>28</sup> The combination of a high lateral resolution and an energy resolution capable of electron spectroscopy for chemical analysis is unprecedented. Apart from switching the light helicity, the use of synchrotron radiation offers the advantage to select the photon energy. In our case, the photon energy is chosen high enough to create excitations into states about 100 eV above  $E_F$  and thus reduces the influence of asymmetries in the excited states around  $E_F$ . The magnetic dichroism occurring in direct photoemission from core or valence-band initial states<sup>11–13</sup> is then used as a magnetic contrast mechanism for imaging magnetic domains. In addition, directly emitted pho-

toelectrons carry information on the chemical state of the specified element.

Magnetic dichroism in photoemission depends on the relative orientation of magnetization, the incident x-ray photons, and the direction of the emitted electrons. Depending on the polarization of the incident photons, two types of magnetic dichroism, i.e., magnetic circular (MCD)<sup>14–18</sup> and magnetic linear (MLDAD) dichroism,<sup>18–25</sup> in the angular distribution of photoelectrons can be distinguished.<sup>11–13</sup> A few experiments have been carried out that use dichroism in core-level photoemission as the contrast mechanism for imaging of magnetic domains.<sup>13,26,27</sup>

In this work, we demonstrate the possibility to study magnetization structures by only considering core-level x-ray photoelectron spectroscopy (XPS) images on a reasonable time scale. While MCD is sensitive to the longitudinal component of the magnetization, MLDAD senses the transverse component of the magnetization.<sup>12,13</sup> We will show that both types of dichroisms can be calculated from just two measurements taken with left and right circular polarization, thus allowing for a quantitative evaluation of magnetization components in a single experimental step. We have chosen as an example a partly recrystallized Fe(100) single crystal at which the well-known simple domain structure within the nonrecrystallized part can be used for normalization in order to demonstrate the numerical evaluation procedure of magnetization patterns.

### II. EXPERIMENTAL SETUP

The spectrometer used for this investigation is a newly designed NanoESCA system that consists of a modified PEEM optics in combination with a band-pass energy filter (double-hemispherical electron analyzer) followed by a de-

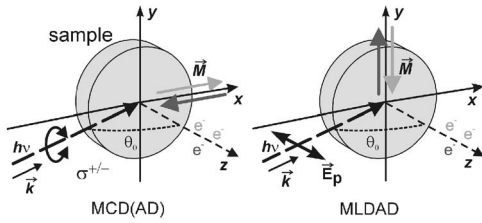


FIG. 1. Geometry of the experiment with sensitivity for the magnetic orientation  $\vec{M}$  (light and dark gray arrows) in the sample. The angle between the incoming beam (in the  $x$ - $z$  plane) and the surface normal  $z$  is  $\theta_0=65^\circ$ .

tection unit consisting of a multichannel plate (MCP) with a screen as well as a CCD (charge coupled device) camera to record the energy-filtered images of the sample surface. The electron optical lenses are all electrostatic. The PEEM immersion lens has an acceptance angle of less than  $\pm 4^\circ$  for electrons with 90 eV kinetic energy and a contrast aperture of 150  $\mu\text{m}$  diameter. Hence in all measurements at this kinetic energy (or higher), only electrons close to the surface normal are detected. With the integration of the band-pass energy filter into the electron optics, it is possible to limit the fraction of the emitted electrons that contribute to a single image to a small range of kinetic energy. Energy scans can be performed over the range of  $0 \leq E_{\text{kin}} \leq 1600$  eV. The energy resolution of the system has been demonstrated to be better than 110 meV, measured at a photon energy of  $h\nu = 83$  eV on the Fermi edge of polycrystalline Cu,<sup>29</sup> and the spatial resolution is better than 120 nm.<sup>28</sup> For the results reported here, the parameters were set to give an energy resolution of  $\Delta E=600$  meV (full width at half maximum) and a spatial resolution of about 200 nm with the field of view set to 75  $\mu\text{m}$ .

The polarization-dependent measurements presented here were performed at the UE52-SGM undulator microspot beamline of the BESSY synchrotron radiation source using circularly polarized radiation with switchable helicity and a high degree of polarization ( $\geq 99\%$ ). The angle of incidence  $\theta_0$  of the photon beam was  $65^\circ$  (with respect to the surface normal). In all images, the photon beam enters from the left side. The geometry of the experiment is depicted in Fig. 1.

For the images presented in this work, we have used a photon energy of  $h\nu=800$  eV in  $\sigma^+$  and  $\sigma^-$  helicity [Fe  $2p_{3/2}$  XPS images, Figs. 2(a) and 2(b)]. The kinetic energy was selected for the maximum contrast for regions A and B.

The sample used in our study was a commercially available polished Fe (100) single crystal that was prepared *in situ* by repeated sputtering and annealing cycles to obtain a clean and well ordered surface. After an annealing procedure just above the Fe fcc-bcc phase-transition temperature, a polycrystalline part showed up in the lower right part of the images that is separated by a sharp boundary along the in-plane [001] axis from the single crystalline area.

### III. EXPERIMENTAL RESULTS

Photoemission intensity maps using the Fe  $2p_{3/2}$  core-level excitation with  $\sigma^+$ -polarized  $\sigma^-$ -polarized light are

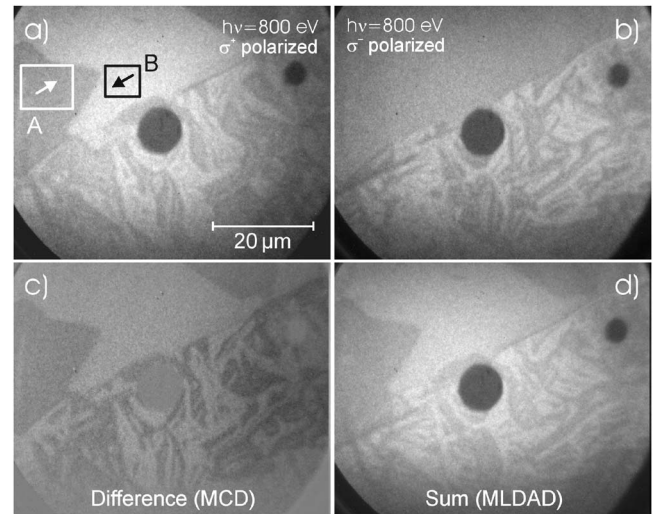


FIG. 2. Photoemission intensity map measured at the Fe  $2p_{3/2}$  core-level, (a) with  $\sigma^+$  polarized light, (b) with  $\sigma^-$  polarized light ( $h\nu=800$  eV). Contrast inversion occurs only in some areas. The bottom row gives (c) the difference image  $I(\sigma^+) - I(\sigma^-)$  and (d) the sum  $I(\sigma^+) + I(\sigma^-)$ . Exposure time is 10 min. The field of view is 75  $\mu\text{m}$ .

shown in Fig. 2. The magnetic domain patterns can be seen at the positive maximum of the asymmetry without any further data processing. To understand the observed patterns, one has to take into account the different dichroism effects: Clearly the MCD is present since circular light is used. The MLDAD occurs due to the  $p$  component of the  $\vec{E}$  vector. The MLD can be neglected at the Fe  $2p$  core level. If the relevant effects are small enough, they will combine linearly.

In the upper part of the image taken with  $\sigma^+$  polarization, a large domain pattern (Fig. 2) with few domains can be seen. The pattern almost disappears in the image with  $\sigma^-$  polarization, indicating that the contrast comprises both MCD and the MLDAD. The MCD changes sign in going from  $\sigma^+$  to  $\sigma^-$  polarization. The disappearing domain pattern in the image with  $\sigma^-$  polarization is due to the compensation of MCD and MLDAD.

The two effects, MCD and MLDAD, can be separated by taking the sum (MLDAD) and the difference (MCD) of the measured maps as shown in Figs. 2(c) and 2(d). In order to quantify this procedure, we assume a linear combination of both effects.<sup>30</sup> From the symmetry it is clear that the MLDAD measures the in-plane component of the magnetization perpendicular to the plane of incidence of the light, i.e., the MLDAD is proportional to  $[\mathbf{k} \times \mathbf{m}] \cdot \mathbf{z}$ , with  $\mathbf{k}$  and  $\mathbf{m}$  denoting unit vectors for the wave vector of the light and the magnetization, respectively. The MCD, instead, is proportional to the magnetization component along  $\mathbf{k}$ , i.e., the MCD is proportional to  $\mathbf{k} \cdot \mathbf{m}$ . Moreover, it changes sign with the helicity of the light. The linear combination of the two effects results in the following intensities:<sup>30</sup>

$$I(\sigma^\pm) = I_0 \{ 1 + c_1([\mathbf{k} \times \mathbf{m}] \cdot \mathbf{z}) \pm c_2 \mathbf{k} \cdot \mathbf{m} \}, \quad (1)$$

where  $c_i(E)$  denote the energy-dependent coefficients of MLDAD and MCD. Using the geometry given in Fig. 1

( $k_y=0$ ), the intensities can be written in the form

$$I(\sigma^\pm) = I_0[1 + c_1 k_x m_y \pm c_c(k_x m_x + k_z m_z)]. \quad (2)$$

Then we define the sum  $I^+$  and difference  $I^-$  of the two measured intensities,

$$I^+ = I(\sigma^+) + I(\sigma^-) = 2I_0(1 + c_1 k_x m_y), \quad (3)$$

$$I^- = I(\sigma^+) - I(\sigma^-) = 2I_0 c_c(k_x m_x + k_z m_z). \quad (4)$$

The definition of the coefficients  $c_i$  is identical to the conventionally defined MLDAD [for  $\mathbf{m}=(0, m_y, 0)$ ] and MCD [for  $\mathbf{m}=(m_x, 0, 0)$ ] asymmetry for two antiparallel magnetization directions along the  $x$  and  $y$  axis, respectively,

$$\frac{I^+(+m_y) - I^+(-m_y)}{I^+(+m_y) + I^+(-m_y)} = c_1 k_x m_y, \quad (5)$$

$$\frac{I^-(+m_x) - I^-(-m_x)}{I^-(+m_x) + I^-(-m_x)} = c_c k_x m_x. \quad (6)$$

The experimental results for intensity maps of  $I^+$  and  $I^-$  are shown in Figs. 2(c) and 2(d). Qualitatively, one sees immediately horizontally and vertically magnetized domains.

For a more quantitative discussion of the magnetization direction, we use the following procedure: First we exploit the known magnetization structure in the upper part of the images where the sample is a single crystal exhibiting a four-fold magnetic anisotropy. Because of the crystalline anisotropy, the magnetization direction will show along a  $\langle 100 \rangle$ -type direction and the minimization of the stray field energy causes the magnetization to be directed in the film plane. An inspection of the domain pattern shown in Figs. 2(c) and 2(d) reveals the magnetization directions as indicated in the figure. The intensities  $I_A^\pm$  and  $I_B^\pm$  from Figs. 2(c) and 2(d) (sum and difference image) measured in the areas corresponding to  $A$  and  $B$  [indicated in Fig. 2(a)] result in the following asymmetries:

$$\frac{I_A^+ - I_B^+}{I_A^+ + I_B^+} = c_1 \sin \theta_0 \sin \phi_M, \quad (7)$$

$$\frac{I_A^- - I_B^-}{I_A^- + I_B^-} = c_c \sin \theta_0 \cos \phi_M. \quad (8)$$

With the known values for the in-plane magnetization direction  $\phi_M$  and the angle of incidence  $\theta_0$  for the photons, we can determine the coefficients  $c_i$ . The additive term  $2I_0$  showing up in the MLDAD can be calculated from the mean value  $2I_0 = (I_A^+ + I_B^+)/2$ . Finally, we determine the magnetization components for each pixel of the image, using the following equations:

$$m_y = \left( \frac{I^+}{2I_0} - 1 \right) \frac{1}{c_1 k_x}, \quad (9)$$

$$m_x = -m_z \cot \theta_0 + \frac{I^-}{2I_0 c_c k_x}. \quad (10)$$

We may assume that because of stray field minimization, the out-of-plane magnetization component  $m_z$  vanishes in our

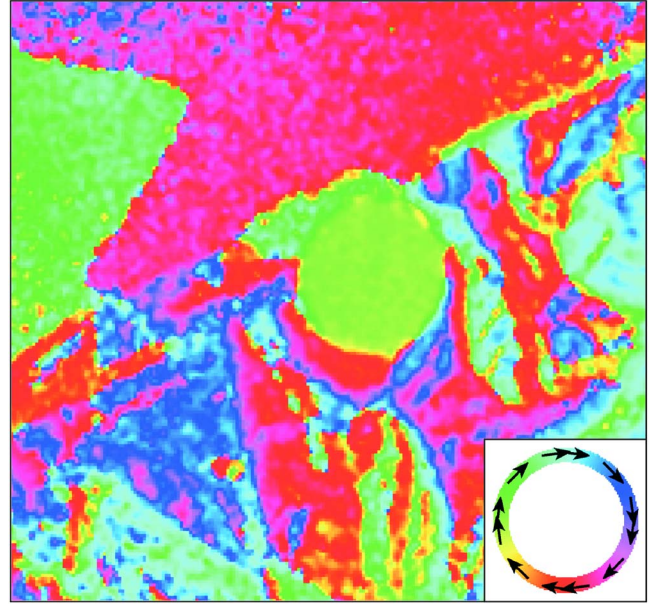


FIG. 3. (Color online) Magnetization structure where the in-plane angle is visualized by the indicated color code as calculated from Figs. 2(c) and 2(d). The image shows a section ( $43 \mu\text{m} \times 40 \mu\text{m}$ ) of the area shown in Fig. 2.

sample.<sup>1</sup> Alternatively, the three magnetization components can be calculated independently from each other, assuming a constant magnetization in the sample, from  $m_x^2 + m_y^2 + m_z^2 = 1$ .

The magnetization structure resulting from this calculation is visualized in Fig. 3, where the in-plane magnetization direction is color-coded. While the domain structure in the upper part of the image Fig. 3 comprises two antiparallely oriented domains, numerous small domains show up in the lower part. A sharp and straight boundary separates the two areas. The magnetization direction is directed parallel to this boundary in the upper part. In the lower part, additional domains with magnetization direction perpendicular to the boundary show up. The circular area in the center of the image, which reveals no magnetic contrast in the photoemission signal because of the low intensity, shows, however, a magnetic contrast in the XMCD signal. The surface in this area is likely covered by a thin layer of a contaminant.

#### IV. DISCUSSION

The polycrystallinity in the lower part of the image can in principle induce an additional morphology or contamination contrast that possibly interferes with the given interpretation. In order to exclude this interference, we also show images using the secondary electron intensity. The photoemission image [Fig. 4(a)] taken at threshold using a UV arc lamp strongly reveals work-function differences and morphology of that sample position. The horizontal white lines in the lower part of the image are due to dislocations and step bunches with a lower work function formed during the recrystallization process. The morphology of the sample surface does not influence the magnetic domain structure, as seen by the XMCD image taken at the same sample position [Fig. 4(b)].

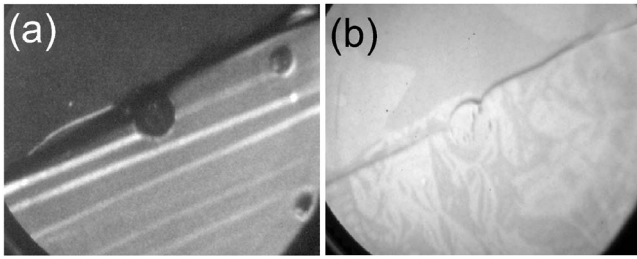


FIG. 4. Photoemission intensity maps of the same sample position as in Fig. 2 measured at the threshold using a uv mercury arc lamp (a) and with secondary electrons ( $E_{\text{kin}}=12.6$  eV) excited by synchrotron light at  $h\nu=708$  eV (Fe  $2p_{3/2}$ ) with  $\sigma^+$  helicity (b). Bright areas correspond to high intensity.

Secondary electron spectra taken at different positions within the image reveal that the circular area in the center of the image shows a higher work function indicating an oxide coverage at this area. The circular contamination area was chosen for reference reasons and appeared very seldom on our sample. Therefore, we can exclude that contaminations contribute to the observed MLD and MCD effect.

The coincidence of the domain patterns seen by the well-known XMCD contrast [Fig. 4(b)] and by the core-level MCD [Fig. 2(c)] confirms our interpretation of domain patterns. The prominent morphology pattern [Fig. 4(a)] is completely absent in the MLDAD image [Fig. 2(d)]. This observation excludes the presence of photoelectron diffraction effects, which generally have to be taken into account when comparing MLDAD signals on differently oriented single-crystal surfaces.<sup>31,32</sup>

A tentative explanation for the observed domain structure can be given by assuming a partial overheating of the sample in the cleaning process. Fe exhibits a structural first-order phase transition from the low-temperature bcc phase to the high-temperature fcc phase at  $T_{\text{cr}}=1185$  K. During the cooling process through  $T_{\text{cr}}$ , dislocations will occur that cause local strains and can influence the magnetic domain structure. While in the upper part of the images the sample obviously remained single crystalline, the lower part has developed a polycrystalline structure. This interpretation is supported by the observation of step bunches in the lower part visible in the uv threshold image shown in Fig. 4(a).

In summary, exploiting the magnetic circular and linear dichroism in the Fe  $2p$  core-level photoemission excitation, we have calculated the magnetization components parallel and perpendicular to the scattering plane independently of each other. The domain structure shows a distinct difference between monocrystalline areas and areas with dislocation lines in an Fe crystal. For the observation of the magnetization structures, we have used a newly developed imaging XPS spectrometer “NanoESCA” with a high spatial resolution capability ( $<200$  nm) exceeding previous approaches for imaging XPS.

#### ACKNOWLEDGMENTS

This work was supported by the BMBF (FKZN 13N7865, 13N7863, 13N7864, 13N7847) and the DFG (SFB 277). We would also like to thank the BESSY staff, and especially F. Senf for his help with the beam-line.

\*Electronic address: elmers@uni-mainz.de

<sup>†</sup>Present address: Universität Würzburg, Experimentelle Physik II, D-97074 Würzburg, Germany.

<sup>1</sup>See, for example, A. Hubert and R. Schäfer, *Magnetic Domains* (Springer, Berlin, 1998).

<sup>2</sup>W. Kuch and C. M. Schneider, Rep. Prog. Phys. **64**, 147 (2001).

<sup>3</sup>S. B. Choe, Y. Acremann, A. Scholl, A. Bauer, A. Doran, J. Stöhr, and H. A. Padmore, Science **304**, 420 (2004).

<sup>4</sup>A. Kuksov, C. M. Schneider, A. Oelsner, A. Krasnyuk, D. Neeb, G. Schönhense, C. de Nadei, and N. B. Brookes, J. Appl. Phys. **95**, 6530 (2004).

<sup>5</sup>P. Fischer, G. Denbeaux, H. Stoll, A. Puzic, J. Raabe, F. Nolting, T. Eimüller, and G. Schütz, J. Phys. IV **104**, 471 (2003).

<sup>6</sup>G. Schütz, W. Wagner, W. Wilhelm, P. Kienle, R. Zeller, R. Frahm, and G. Materlik, Phys. Rev. Lett. **58**, 737 (1987).

<sup>7</sup>J. Stöhr, J. Electron Spectrosc. Relat. Phenom. **75**, 253 (1995).

<sup>8</sup>C. T. Chen, Y. U. Idzerda, H.-J. Lin, N. V. Smith, G. Meigs, E. Chaban, G. H. Ho, E. Pellegrin, and F. Sette, Phys. Rev. Lett. **75**, 152 (1995).

<sup>9</sup>E. Bauer, J. Phys.: Condens. Matter **13**, 11391 (2001).

<sup>10</sup>B. P. Tonner, D. Dunham, J. Zhang, W. L. O'Brien, M. Samant, D. Weller, B. D. Hermsmeier, and J. Stöhr, Nucl. Instrum. Methods Phys. Res. A **347**, 142 (1994).

<sup>11</sup>H. Ebert, L. Baumgarten, C. M. Schneider, and J. Kirschner,

Phys. Rev. B **44**, 4406 (1991).

<sup>12</sup>J. Henk, A. M. N. Niklasson, and B. Johansson, Phys. Rev. B **59**, 13986 (1999).

<sup>13</sup>W. Kuch, L. I. Chelaru, F. Offi, M. Kotsugi, and J. Kirschner, J. Vac. Sci. Technol. B **20**, 2543 (2002).

<sup>14</sup>W. Kuch, A. Dittschar, K. Meinel, M. Zharnikov, C. M. Schneider, J. Kirschner, J. Henk, and R. Feder, Phys. Rev. B **53**, 11621 (1996).

<sup>15</sup>D. Venus, Phys. Rev. B **56**, 2661 (1997).

<sup>16</sup>L. Baumgarten, C. M. Schneider, H. Petersen, F. Schäfers, and J. Kirschner, Phys. Rev. Lett. **65**, 492 (1990).

<sup>17</sup>F. U. Hillebrecht, Ch. Roth, H. B. Rose, M. Finazzi, and L. Braicovich, Phys. Rev. B **51**, 9333 (1995).

<sup>18</sup>J. Bansmann, L. Lu, K. H. Meiwes-Broer, T. Schlathölter, and J. Braun, Phys. Rev. B **60**, 13860 (1999).

<sup>19</sup>Ch. Roth, F. U. Hillebrecht, H. B. Rose, and E. Kisker, Phys. Rev. Lett. **70**, 3479 (1993).

<sup>20</sup>F. Sirotti and G. Rossi, Phys. Rev. B **49**, 15682 (1994).

<sup>21</sup>G. Rossi, G. Panaccione, F. Sirotti, and N. A. Cherepkov, Phys. Rev. B **55**, 11483 (1997).

<sup>22</sup>W. Kuch, M.-T. Lin, W. Steinhögl, C. M. Schneider, D. Venus, and J. Kirschner, Phys. Rev. B **51**, 609 (1995).

<sup>23</sup>H. B. Rose, Ch. Roth, F. U. Hillebrecht, and E. Kisker, Solid State Commun. **91**, 129 (1994).

- <sup>24</sup>D. Venus, W. Kuch, M.-T. Lin, C. M. Schneider, H. Ebert, and J. Kirschner, *Phys. Rev. B* **55**, 2594 (1997).
- <sup>25</sup>A. Rampe, G. Güntherodt, D. Hartmann, J. Henk, T. Scheunemann, and R. Feder, *Phys. Rev. B* **57**, 14370 (1998).
- <sup>26</sup>C. M. Schneider, Z. Celinski, M. Neuber, C. Wilde, M. Grunze, K. Meinel, and J. Kirschner, *J. Phys.: Condens. Matter* **6**, 1177 (1994).
- <sup>27</sup>C. M. Schneider, *J. Magn. Magn. Mater.* **175**, 160 (1997).
- <sup>28</sup>M. Escher, N. Weber, M. Merkel, C. Ziethen, P. Bernard, G. Schönhense, S. Schmidt, F. Forster, F. Reinert, B. Krömker, and D. Funnemann, *J. Phys.: Condens. Matter* **17**, S1329 (2005).
- <sup>29</sup>M. Escher, N. Weber, M. Merkel, B. Krömker, D. Funnemann, S. Schmidt, F. Reinert, F. Forster, S. Hüfner, P. Bernhard, C. Ziethen, H. J. Elmers, and G. Schönhense, *J. Electron Spectrosc. Relat. Phenom.* **144-147**, 1179 (2005).
- <sup>30</sup>G. van der Laan, *Phys. Rev. B* **51**, 240 (1995).
- <sup>31</sup>R. Schellenberg, E. Kisker, A. Fanelis, F. U. Hillebrecht, J. G. Menchero, A. P. Kaduwela, C. S. Fadley, and M. A. Van Hove, *Phys. Rev. B* **57**, 14310 (1998).
- <sup>32</sup>F. Bruno, G. Panaccione, A. Verdini, R. Gotter, L. Floreano, P. Torelli, M. Sacchi, F. Sirotti, A. Morgante, and G. Rossi, *Phys. Rev. B* **66**, 024417 (2002).